Protein Science (1999), *8*:778–787. Cambridge University Press. Printed in the USA.

Nucleotide binding to the G12V-mutant of Cdc42 investigated by X-ray diffraction and fluorescence spectroscopy: Two different nucleotide states in one crystal

MARKUS GEORG RUDOLPH, ALFRED WITTINGHOFER, AND INGRID RENATE VETTER

Max-Planck Institut für molekulare Physiologie, Abteilung Strukturelle Biologie, Rheinlanddamm 201, 44139 Dortmund, Germany

(RECEIVED October 2, 1998; ACCEPTED December 31, 1998)

Abstract

The 2.5 Å crystal structure of the full length human placental isoform of the Gly12 to Val mutant Cdc42 protein (Cdc42(G12V)) bound to both GDP/Mg^{2+} and $GDPNH_2$ (guanosine-5′-diphospho-β-amidate) is reported. The crystal contains two molecules in the asymmetric unit, of which one has bound GDP/Mg^{2+}, while the other has bound $GDPNH_2$ without a Mg^{2+} ion. Crystallization of the protein was induced via hydrolysis of the Cdc42·GppNHp complex by the presence of contaminating alkaline phosphatase activity in combination with the crystallization conditions. This prompted us to compare the binding characteristics of $GDPNH_2$ vs. GDP. The amino group of $GDPNH_2$ drastically reduces the affinity to Cdc42 in comparison with that of GDP, causes the loss of the Mg^{2+} ion, and apparently also increases the conformational flexibility of the protein as seen in the crystal. Both the switch I and switch II regions are visible in the electron density of the GDP-bound molecule, but not in the molecule bound to $GDPNH_2$. The C-terminus containing the CaaX-motif is partly ordered in both molecules due to an intramolecular disulfide bond formed between Cys105/Cys188 and Cys305/Cys388, respectively.

Keywords: crystallography; fluorescence; mant-nucleotides; nucleotide analogues; nucleotide binding; Rho-family; small GTPases

Members of the Rho-family of Ras-related GTP binding proteins, namely Rho, Rac, and Cdc42, are involved in the regulation of the actin cytoskeleton (Nobes & Hall, 1995). Like Ras, they function as molecular switches cycling between a biologically inactive GDP-bound state and an active GTP-bound state. The relative abundance of these states is regulated by guanine nucleotide exchange factors (GEFs) and GTPase activating proteins (GAPs) (Bourne et al., 1990). In the GTP-bound state, they interact with effectors that are defined as molecules having a high affinity to the GTP bound state as opposed to a low affinity to the GDP-bound state.

Structures of Rac complexed to a GTP analogue, Rac1·GppNHp (Hirshberg et al., 1997) and of RhoA·GDP (Wei et al., 1997) and RhoA·GTPγS (Ihara et al., 1998) have been solved by X-ray crystallography and showed interesting variations in the nucleotide binding site. An NMR structure of Cdc42 in both the GDP and $GppCH_2p$ (guanosine-5′-(β,γ-methylene)triphosphate) form was reported and showed the switch regions to be disordered (Feltham et al., 1997). Furthermore, a complex between RhoGAP and either Cdc42·GppNHp in the ground state or RhoA·GDP·AlF_4^- in the transition state has recently been reported, but without mentioning details of the nucleotide binding site (Rittinger et al., 1997a, 1997b). While some of these structures are of the truncated versions of the GTP-binding proteins, which lack the C-terminal end containing the CaaX box and the motifs for posttranslational modification, other structures did not show density for this region. In our efforts to understand differences in nucleotide binding properties and to understand the contribution of the C-terminus, we sought to crystallize the full length Cdc42 protein complexed to GppNHp. Serendipitously, crystals of full-length Cdc42(G12V) in the GDP-bound form as well as with the GDP-analogue $GDPNH_2$ were obtained, which brought interesting insights into nucleotide and Mg^{2+}-binding properties as well as the structure of the C-terminal extension.

Reprint requests to: Ingrid Renate Vetter, Max-Planck Institut für molekulare Physiologie, Abteilung Strukturelle Biologie Rheinlanddamm 201, 44139 Dortmund, Germany; e-mail: ingrid.vetter@mpi-dortmund.mpg.de.

Abbreviations: Cdc42(G12V), G12V mutant of human placental Cdc42; GppNHp, guanosine-5′-(β,γ-imido)triphosphate; $GDPNH_2$, guanosine-5′-diphospho-β-amidate; mant, N-methyl-anthraniloyl-; mGDP, 2′- and 3′-O-(N-methylanthraniloyl)-guanosine diphosphate.

Results

Overall structure

Crystals were grown from solutions of Cdc42(G12V)·GppNHp and analyzed for nucleotide content. Surprisingly, HPLC analysis

of dissolved crystals showed a 1:1 ratio of GDP and $GDPNH_2$ instead of GppNHp. These results will be discussed in detail below. The asymmetric unit contains two molecules of Cdc42(G12V) whose overall structure shows the expected topology of the Ras protein, namely an open twisted β-sheet flanked by α-helices (Fig. 1). The two proteins form a dimer with a twofold noncrystallographic symmetry and a buried surface area of 700 $Å^2$ per monomer (1.7 Å probe radius; Connolly, 1993). Only 15 specific interactions stabilize the dimer in the crystals, which apparently is not sufficient for significant dimerization of Cdc42 in solution as judged from gel filtration studies (M. Rudolph, unpubl. obs.). As expected from the high sequence homology, the structure of Cdc42(G12V) is very similar to Rac1 (81% similarity) and RhoA (70% similarity). A comparison of the coordinates of the Rac1·GppNHp (PDB entry 1mh1) and the RhoA·GDP structure (PDB entry 1ftn) with Cdc42(G12V) shows a root-mean-square deviation (RMSD) of only 0.94 Å (165 Cα-atoms) and 1.16 Å (171 Cα-atoms), respectively (Fig. 2). In contrast, the NMR structure of Cdc42 (PDB entry 1aje) superimposes with the crystal structure of Cdc42(G12V) with an RMSD of 4.26 Å (178 Cα-atoms) mainly because of drastic differences in the switch regions, the insert region, and the C-terminal part (see below). Omitting these regions for comparison, the core turns out to be quite similar with 122 Cα-atoms overlaying with an RMSD of 1.88 Å.

The major difference between Rho proteins and other subfamilies of Ras-related proteins is an insertion of 13 residues between β5 and α4, which adopts a helical structure. Since coordinates of none of the Rho-family members were available when the structure determination was in progress, Ras (PDB entry 4q21) had to be used as the model for molecular replacement. The presence of electron density for the insert region is therefore a proof for the validity of the structure determination of Cdc42(G12V). The insert region (encompassing residues Ile117 to Ile137) adopts the same helical conformation and position as in RhoA·GDP and Rac1·GppNHp. The insert region is only visible in molecule 1, and not in molecule 2. In molecule 1, the insert helix is solvent exposed and has almost no contacts with symmetry-related molecules, which is consistent with the high *B*-factors in this part of the molecule. This is in line with the situation in the Rac1·GppNHp structure where this region is found to have higher *B*-factors as well. In contrast, the insert region in the RhoA·GDP structure packs tightly against symmetry-related molecules, thus explaining the lower *B*-factors in this structure.

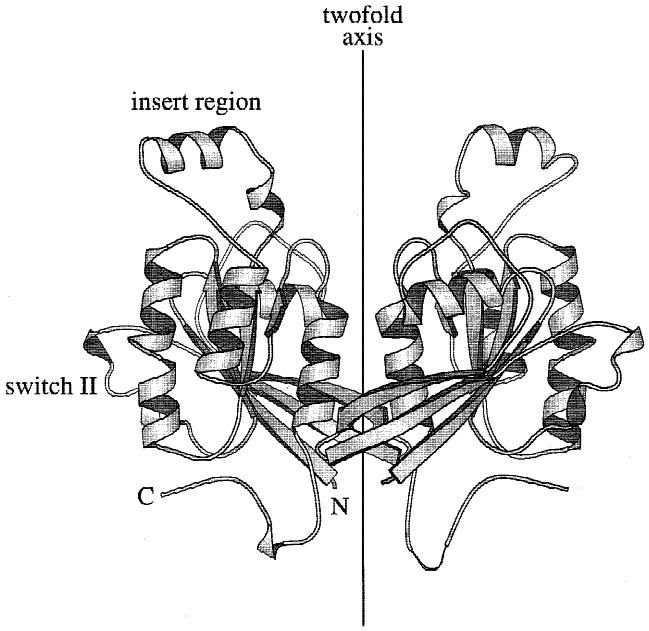

Fig. 1. Overall structure of the asymmetric unit of Cdc42(G12V). Indicated are the twofold noncrystallographic axis, the termini, the insert region, and the switch II region. The figure was drawn using MOLSCRIPT (Kraulis, 1991).

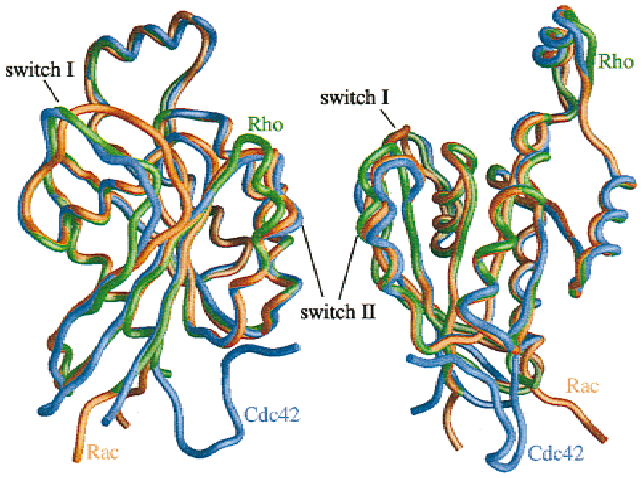

Fig. 2. Overlay of Cdc42(G12V) (blue) with Rac1·GppNHp (red) and RhoA·GDP (green). **Left:** Cα-trace stressing the differences in structure of the switch I regions. The switch II region and the insert region are very similar independent of the nucleotide state. **Right:** View rotated 90° compared to left. The figure was drawn with GRASP (Nicholls et al., 1991).

Nature of the substrates and nucleotide affinity

In the original electron density generated from the starting model without nucleotide and Mg^{2+}, no density was identified that could be interpreted as a γ-phosphate. Instead, GDP and Mg^{2+} were found in the active site of the first molecule. Furthermore, density for neither a γ-phosphate nor a Mg^{2+} at the corresponding position was observed in the second molecule of the asymmetric unit. These features were puzzling and prompted us to investigate the nucleotide composition in the crystals. High-performance liquid chromatography (HPLC) analysis of crystals revealed a 1:1 ratio of the nucleotides GDP and $GDPNH_2$ as shown in Figure 3 in comparison with appropriate marker nucleotides. The peaks have identical areas but differ in shape. The peak of $GDPNH_2$ is very sharp and well resolved, whereas the GDP peak is broader indicating a slower dissociation of GDP than $GDPNH_2$ from the Cdc42(G12V)·nucleotide complex under the conditions of the HPLC. Since the two molecules in the asymmetric unit show differences in the active site (see below) and the observed GDP/$GDPNH_2$ ratio is 1:1, we have to assume that one molecule is bound to GDP/Mg^{2+}, while the other is bound to $GDPNH_2$. This finding is further corroborated by the fact that the Cdc42(G12V)·GDP complex did not crystallize, whereas Cdc42(G12V)·GDP supplemented with a mixture of GDP and $GDPNH_2$ yielded crystals (although

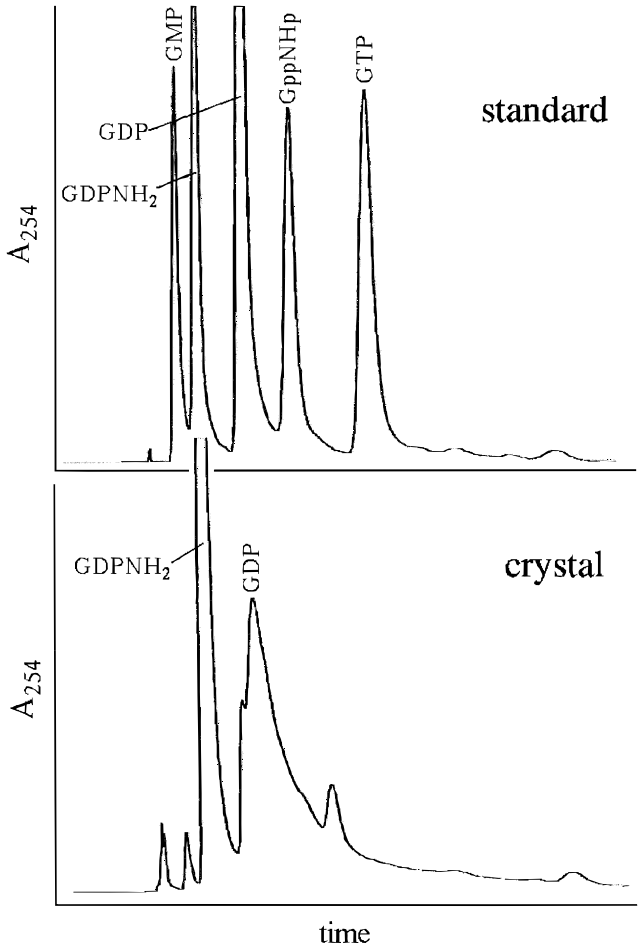

Fig. 3. HPLC analysis of a Cdc42(G12V)·nucleotide crystal. A crystal grown under the same conditions and of the same age as the one from which the native data set was collected was dissolved and subjected to isocratic HPLC analysis as described under Materials and methods. Upper panel: standard of (increasing retention times) GMP, $GDPNH_2$, GDP, GppNHp, GTP. Lower panel: crystal. Note the differences in shape but the equal areas of the GDP and $GDPNH_2$ peaks.

small), stressing the importance of the asymmetry in the active sites for successful crystallization.

Ras and other GTP-binding proteins have been successfully crystallized as GppNHp complexes. To address the question as to how the Cdc42(G12V)-bound GppNHp got decomposed into GDP and $GDPNH_2$, solutions of Cdc42(G12V)·GppNHp were checked for activities hydrolyzing the supposedly nonhydrolyzable GTP analogue.

First, the Cdc42(G12V) preparation was assayed for contaminating phosphatase activity since GppNHp complexes were prepared by exchanging the originally bound GDP against GppNHp using soluble alkaline phosphatase (John et al., 1990). This enzyme, known to hydrolyze GDP, but not GppNHp, drives the exchange reaction toward completion (John et al., 1988). Yet, a control experiment showed that prolonged incubation of GppNHp with alkaline phosphatase at ambient temperature and neutral pH results in the cleavage of GppNHp into GDP, GMP, and guanosine. It turns out that the solutions of Cdc42(G12V)·GppNHp purified according to our standard protocol (John et al., 1988) contained trace amounts of phosphatase activity. It remains unclear as to why the separation of alkaline phosphatase and Cdc42(G12V) has not been achieved in spite of a gel filtration step after the exchange reaction. Thus, it is most likely that the GDP is produced by enzymatic hydrolysis of GppNHp due to traces of alkaline phosphatase in the protein preparation.

Second, a control experiment showed that GppNHp is cleaved and almost quantitatively converted into $GDPNH_2$ in the protein-free crystallization solution itself (0.1 M NaOAc pH 4.7, 5% PEG 4000, 0.3 M Li_2SO_4). This degradation occurs in a time span of several days and yields only $GDPNH_2$ but no other degradation products (~90% of the GppNHp is converted to $GDPNH_2$ within 3 weeks). The presence of 0.3 M Li_2SO_4 leads to a drastic increase in the dissociation rate constant (data not shown) of both GDP and GppNHp from Cdc42(G12V) (3.5×10^{-3} s^{-1} and 12.0×10^{-3} s^{-1}, respectively) as compared to the absence of Li_2SO_4 (2.0×10^{-5} s^{-1} and 39.0×10^{-5} s^{-1}, respectively), which means that the nucleotides are more easily accessible to the phosphatase.

Since the β-phosphate is considered to be an important element of the tight binding of guanine nucleotides to Ras-related proteins (John et al., 1990; Rensland et al., 1995), we wondered how the reduction of negative charge on the β-phosphate would influence the binding characteristics under physiological buffer conditions. Figure 4A shows that the dissociation rate constant of $GDPNH_2$ (0.34 s^{-1}) in 40 mM HEPES/NaOH pH 7.4, 100 mM NaCl, 5 mM $MgCl_2$ is 10,000-fold faster than that of GDP (0.33×10^{-4} s^{-1}). In the case of Ras, it was found that any modification of the nucleotide or of the protein does not affect the association rate constant significantly, but only the dissociation rate (Rensland et al., 1995). Assuming the same for Cdc42(G12V), the binding constant for $GDPNH_2$ should be greatly reduced as well. Direct titration of $GDPNH_2$ to nucleotide-free Cdc42(G12V) using intrinsic protein fluorescence as a probe (Fig. 4B) yielded a relatively large equilibrium dissociation constant of $K_d = 0.22 \pm 0.056$ μM (three independent measurements). The affinity of GDP to nucleotide-free Cdc42(G12V), however, was too high to be measured by titration. Kinetic determination of K_d for the Cdc42(G12V)·GDP complex as the ratio of the rate constants for the dissociation and association reactions ($k_{ass} = 3.5 \times 10^6$ M^{-1} s^{-1} for mGDP, data not shown) yielded a $K_d = 9.4$ pM, which, within the experimental error, compares well with the difference in dissociation constants of the Cdc42(G12V)·nucleotide complexes mentioned above.

Mg^{2+} binding, nucleotide binding, and P-loop

Figures 5A and 5B show an omit map around the nucleotide sites of the two molecules in the asymmetric unit. For Cdc42(G12V)·GDP, the Mg^{2+} is coordinated essentially like in the Ras·GDP structure (Milburn et al., 1990; Tong et al., 1991) with the side chain of Thr17 (Ser17 in Ras), one β-phosphate oxygen, and four water molecules as ligands of the first coordination sphere forming a distorted octahedron as one of the axial water molecules (H_2O 1,000 in Fig. 5A,C) is not in line with the Mg^{2+} and the other axial ligand (a β-phosphate oxygen), but is offset by an angle of approximately 45°. Its position is stabilized by three hydrogen bonds with the side chain of Thr17, the side chain of Asp57, and an equatorial water molecule complexed to the Mg^{2+} (Fig. 5C). The space that results from the shift of the axial water molecule (H_2O 1,000 in Fig. 5A,C) is occupied by the side chain of Phe37, which is located closer to the interior of the mol-

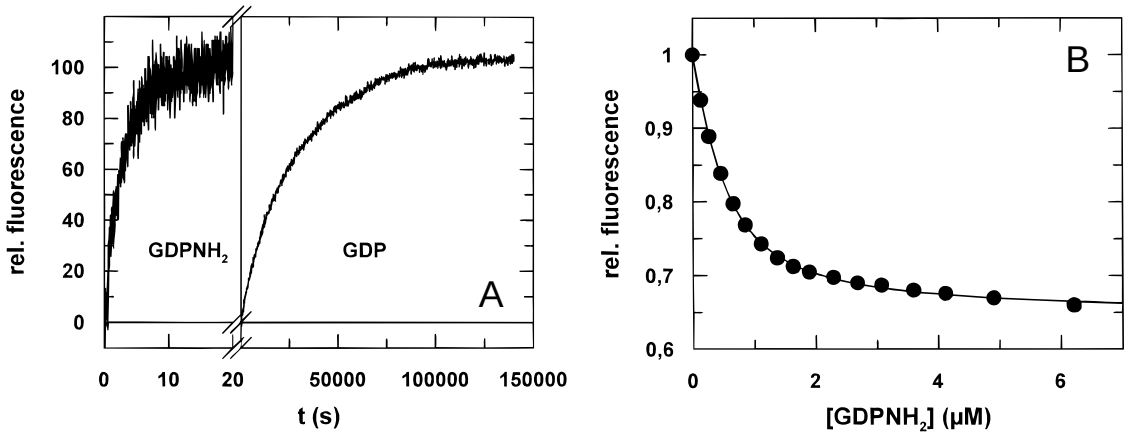

Fig. 4. Dissociation of Cdc42(G12V)·nucleotide complexes (**A**) and fluorescence titration of $GDPNH_2$ to nucleotide-free Cdc42(G12V) (**B**). **A:** 0.1 μM nucleotide free Cdc42(G12V) in 40 mM HEPES/NaOH pH 7.4, 100 mM NaCl, 5 mM $MgCl_2$ was preincubated with 2 μM $GDPNH_2$ and dissociated with 5 μM mGDP in a stopped flow apparatus (left panel); 0.14 μM Cdc42(G12V)·GDP was dissociated by addition of 4.2 μM mGDP (right panel). Fluorescence was excited at 295 nm and the increase in fluorescence due to energy transfer from Trp97 to the mant moiety measured at 435 nm. The amplitudes of the spectral increases were normalized. Single exponentials were fit to the data yielding apparent dissociation rate constants of 0.34 s^{-1} for $GDPNH_2$ and 0.33 $\times$ 10^{-4} s^{-1} for GDP, respectively. **B:** 0.4 μM nucleotide-free Cdc42(G12V) in 40 mM HEPES/NaOH pH 7.4, 100 mM NaCl, 5 mM $MgCl_2$ was titrated with increasing concentrations of $GDPNH_2$. The decrease in tryptophan fluorescence of Cdc42(G12V) was followed at 328 nm after excitation at 295 nm. The solid curve represents the best fit of an equation describing a simple binding equilibrium to the data and yields a dissociation constant of 0.3 μM.

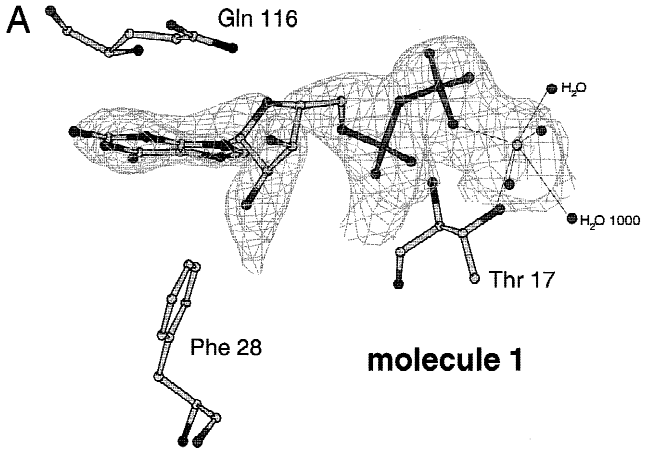

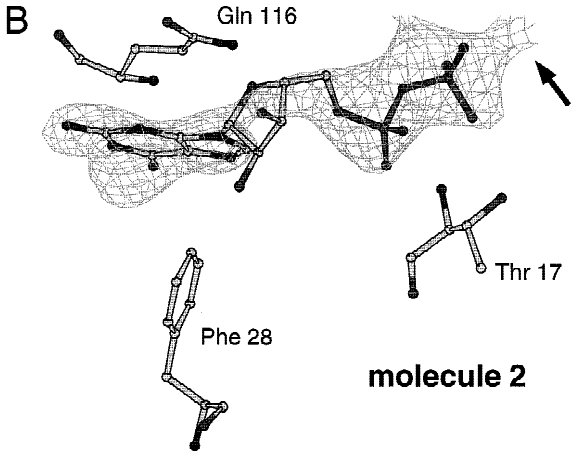

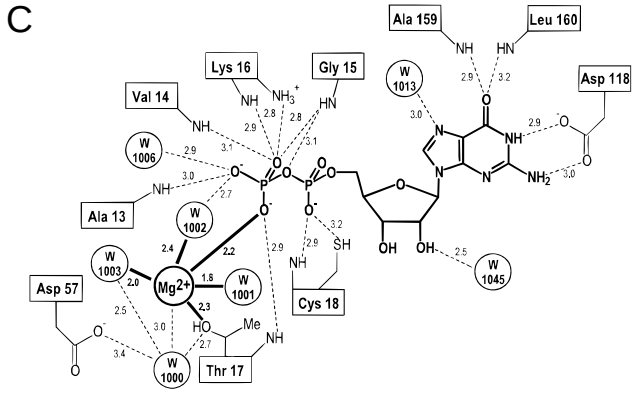

Fig. 5. Omit maps of the nucleotide binding sites and selected side chains of the environment of GDP. **A, B:** $F_o - F_c$ omit map calculated after simulated annealing refinement of the final model without nucleotides and Mg^{2+} cut at the 2σ level showing the presence of the substrates GDP and $GDPNH_2$ as well as the asymmetric distribution of the Mg^{2+} ion. Density for the Mg^{2+} ion is present only in the first molecule (**A**), whereas in the second molecule an additional stretch of density (arrow) is visible around the putative position of the nitrogen atom (**B**). **C:** Schematic plot of the residues interacting with GDP in molecule 1. Panels A and B were produced with BOBSCRIPT (Esnouf, 1997).

ecule compared to Glu37 in Ras and Phe37 in Rac1. Interestingly, in the RhoA·GDP structure this coordination site is occupied by the carbonyl oxygen of Thr37. The corresponding Thr35 in Cdc42(G12V) hydrogen bonds to Asp63 of a symmetry-related molecule. Therefore, neither the side-chain nor the main-chain carbonyl is available for interaction with the Mg^{2+}.

A superposition of the models of Ras and Cdc42(G12V)·GDP reveals a very similar position of the nucleotide. A distinguishing feature of the Rho/Rac/Cdc42 subfamily is a degeneration of the NKxD sequence motif of GTP-binding proteins to [T,N][K,Q]xD. Most of these proteins contain a threonine instead of asparagine, and Cdc42 and TC10 have a glutamine instead of the lysine. In the Cdc42(G12V) structure, the glutamine packs against the guanine base like the equivalent lysine in Ras (Fig. 5A,B). Thus, only two methylene groups of the side chain (as opposed to four in lysine) are available for hydrophobic interaction with the guanine base. An additional consequence is the loss of a hydrogen bond between Lys117 in Ras (which is Gln116 in Cdc42) and the main-chain carbonyl of Gly13 in the P-loop. The other interactions of Cdc42(G12V) with the guanine base, involving the invariant Phe28, Asp118 (Asp119 in Ras), and Ala159 (Ala146 in Ras) are as expected from Ras-related GTP-binding proteins (Fig. 5).

The second molecule in the asymmetric unit, which is bound to $GDPNH_2$, shows some interesting differences compared to the first molecule, which is bound to GDP/Mg^{2+}. The Cdc42(G12V)·$GDPNH_2$ molecule shows somewhat longer distances between the oxygen atoms and the main-chain NH groups. Although this observation has to be interpreted with caution due to the less well-defined density for this molecule, this difference was observed consistently in spite of the application of NCS-constraints and thus appears to be significant. The same argument holds for an $F_o - F_c$ map at a cut-off of 2σ, which shows additional density in molecule 2 stretching from the β-phosphate via two putative water molecules toward Ala259 in the switch II region (arrow in Fig. 5B). This could indicate a putative water mediated hydrogen bond to the NH_2 group of $GDPNH_2$, which would fix the position of the NH_2 group.

The structure described contains the G12V mutation, which has been shown to block both the intrinsic and RhoGAP-mediated GTPase activity (Lancaster et al., 1994; Ahmadian et al., 1997) and has been used in microinjection and transfection experiments as constitutively active gene for filopodia induction and cell transformation (Nobes & Hall, 1995; Olson et al., 1996; Qiu et al., 1997). The P-loops of mutant Cdc42(G12V)·GDP, RhoA·GDP, and Rac1·GppNHp overlay without significant deviation leading to the conclusion that the G12V mutation does not alter the conformation of the P-loop in Cdc42(G12V)·GDP, supporting the argument put forward for the homologous mutations found in Ras oncogenes that even large side chains in position 12 of the P-loop do not alter the structure per se (Krengel et al., 1990; Tong et al., 1991; Franken et al., 1993).

Trp97 and fluorescence studies

A peculiarity of the Rho-family protein structures determined so far is the presence of a kink in helix α3, at residue Glu95 in Cdc42 (Fig. 6). The corresponding helix in Ras does not show this feature. Glu95 is looped out in the middle of the long α-helix, and Lys96 in Cdc42(G12V)·GDP and Gln95 in Ras as well as Asn92 (Cdc42) and Asp92 (Ras) are structurally equivalent. This presumably energetically unfavorable helix insertion (Sondek & Shortle, 1990; Vetter et al., 1996) is probably stabilized by flanking residues, which are deeply buried in the hydrophobic core, namely Trp97, a residue that is invariant among the Rho-family members, Val93 (Ile95 in RhoA), and Ile101 (Val103 in RhoA). Trp97 is sandwiched hydrophobically between the side chains of Val9 and Lys96, which lock the indole ring in a rigid conformation (Fig. 6). On the N-terminal side of the looped-out Glu95, Val93 is intimately involved in hydrophobic interactions with Val80, Phe82, Phe90, Leu112, Leu145, and Leu149. C-terminal to Glu95, Ile101 is part of a hydrophobic core with Tyr72, Phe78, Val98, and Phe110 (Fig. 6).

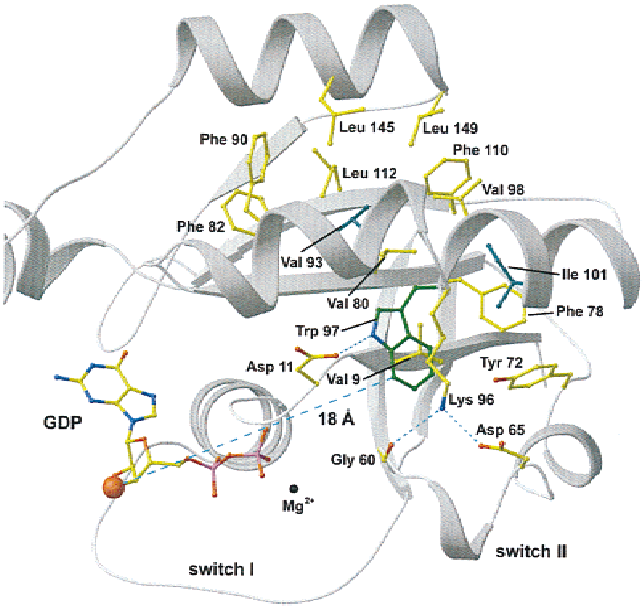

Fig. 6. Spatial arrangement of Trp97 and the nucleotide explaining the observed fluorescence behavior of Cdc42. The indole ring is in the hydrophobic core of Cdc42 and within 18 Å distance from the ribose moiety of GDP, which carries the mant group (red ball) in fluorescent nucleotides. Residues Val9 and Lys96 sandwiching Trp97 (green) are outlined. On the N- and C-terminal side of the discontinuity in helix α3 Val93 and Ile101 are highlighted in cyan and residues hydrophobically interacting with them are outlined in yellow. The figure was drawn with BOBSCRIPT (Esnouf, 1997) and rendered with Raster3D (Merrit & Bacon, 1997).

Additionally to its hydrophobic interactions, Trp97 is surrounded by a hydrogen bond network made up by Glu100, Arg68, Gly60, Asp11, and Asn92. As shown by tryptophan fluorescence quenching and fluorescence emission spectra, the environment of Trp97 is not totally solvent inaccessible (Leonard et al., 1994), which is in accordance with the position of Trp97 in the structure. Trp97 is about 18 Å away from the ribose moiety of the nucleotide (Fig. 6), a distance that is well within the range where fluorescence energy transfer from tryptophan to the mant group can occur. The almost total quenching of the tryptophan fluorescence by a mant group bound to the ribose can conveniently be explained by the rigid conformation the Trp97 side chain adopts in the structure.

The fluorescence of Trp97 was shown to be sensitive to the nucleotide state of Cdc42 (Leonard et al., 1994). However, the surroundings of the Trp97 are not significantly different in the Cdc42(G12V)·GDP and the Rac1·GppNHp structures. Since NMR studies have detected chemical shift changes in the region of Trp97 upon change of the nucleotide state from GDP to $GppCH_2$ (Feltham

et al., 1997), these changes have to be either very subtle or are suppressed in the crystal structures.

Structure of the C-terminal end

In the structure of full-length Cdc42(G12V)·GDP reported here, the C-terminal 13 amino acids are partly visible in the electron density, probably due to a stabilizing disulfide bond between Cys105 and Cys188. Electro spray mass spectrometry has shown that a shortened construct of Cdc42(G12V) lacking the CaaX motif readily reacts with β-mercaptoethanol and glutathione (M. Rudolph, unpubl. obs.). Since all other Cys residues (Cys6, Cys18, Cys81) are buried inside the hydrophobic core of the protein, it appears that Cys105 is the reactive cysteine residue in these experiments as well. Cys105 is conserved among the Rho-family and positioned at the C-terminal end of an α-helix (α3) where usually only a small effect on the pK_a value of a cysteine residue is observed (Kortemme & Creighton, 1995). However, Cys105 is preceded in sequence by two histidine residues that might increase the reactivity of the cysteine, similar to the reactive cysteine in protein tyrosine phosphatases (PTPs) (Fauman & Saper, 1996) or enzymes of the fatty acid synthetase or thiolase family (Huang et al., 1998), all of which work via nucleophilic attack of a thiolate and formation of a thiolated enzyme intermediate. As a result of the disulfide bond, the C-terminal end is strongly bent. A number of interactions between the C-terminal end and the main body of the G-domain stabilize this region but the structure of the G domain itself is not perturbed as compared to RhoA·GDP or Rac1·GppNHp. Why the Rho-family members conserve an apparently hyperreactive cysteine residue (Cys105) that leads to artificial disulfide formation in vitro is not clear at present.

Comparison of the switch regions of Cdc42(G12V) to Ras, RhoA, and Rac1

In Ras, the regions comprising residues 32–40 and 60–74 have been called effector (switch I) and switch II regions, respectively, because they undergo major structural rearrangements during GTP hydrolysis. Mutations in the switch I region block the biological effect of Ras, and indeed, the structure of the complex between the Ras homologue Rap and the effector Raf has shown that these residues are involved in the interaction with effectors (Nassar et al., 1995, 1996). For Rho-type GTP-binding proteins, the same region also participates in binding to their specific effectors and is involved in defining the specificity of interaction (Best et al., 1996; Matsui et al., 1996; McCallum et al., 1996; Quilliam et al., 1996; Li & Zheng, 1997). In the Cdc42(G12V) crystal, both switch regions are clearly defined in molecule 1 but not visible in molecule 2. Figure 2 compares molecule 1 of Cdc42(G12V)·GDP with the structures of Rac1·GppNHp and RhoA·GDP and depicts the different positions of the effector loops.

The detailed conformation of the Cdc42(G12V)·GDP loop 1 (residues Tyr32 to Tyr40, defined in analogy to Ras) differs from the Ras·GDP loop, which is not surprising because of the considerably different sequences. However, the canonical structural change of Ras upon nucleotide exchange, where Thr35 contacts the Mg^{2+} in the GppNHp form, is observed in Cdc42 as well, as shown by the structure of Cdc42·GppNHp in complex with RhoGAP (Rittinger et al., 1997a).

In spite of the high sequence similarity, the effector loop of Cdc42(G12V)·GDP also differs from the RhoA·GDP structure (Fig. 2). The most pronounced conformational change between Cdc42(G12V) and RhoA occurs at the side chain of Phe37 (Phe39 in RhoA), which packs against other residues of the effector loop in RhoA, whereas in Cdc42(G12V) it is stretched out toward the switch II region. The sequence from Pro29 to Pro34 in Cdc42(G12V)·GDP overlays well with the corresponding region Pro31 to Pro36 in RhoA·GDP. In both the Rho·GDP and the Cdc42(G12V)·GDP structure, crystal packing is probably involved in fixing the effector loop. However, the conformation of the switch I region of Cdc42(G12V) is not solely stabilized by crystal contacts. Ser30 hydrogen bonds via a water molecule with the carbonyl oxygen of Phe28 and the side chain of Tyr32 is held in position by an intramolecular hydrogen bond with the hydroxyl group of Thr35. A hydrophobic cluster is formed by the side chains of Cys18, Ile21, Phe28, Pro29, and Pro34.

The switch I region or effector loop of Rac1·GppNHp shows poor density (Hirshberg et al., 1997). The maximum distance of Cα-atoms in this region between Cdc42(G12V)·GDP and Rac1·GppNHp is 7.6 Å (Pro34), underlining the large conformational change of the effector loop atoms (for Rac1 a partly occupied conformation for residues 32–36 in the crystal structure was taken). In contrast to Cdc42(G12V), the effector loop of Rac1 has almost no crystal packing contacts. It is, therefore, not clear whether the difference in conformations is due to the different nucleotide states or to the crystal contacts in the Cdc42(G12V) structure. No structural comparison could be done for the solution and crystal structures of Cdc42 because in the NMR structure of Cdc42 the switch I region was not tightly constrained and suggested to be mobile (Feltham et al., 1997).

The switch II region (residues 60 to 70) differs from that in Ras·GDP and adopts a helical conformation almost identical to the one in Rac1·GppNHp (RMSD 0.96 Å within 11 Cα atoms, Fig. 2) and RhoA·GDP (2.1 Å within 8 Cα atoms since residues 63–65 are disordered). This is in contrast to the situation in solution where no helical assignment for the switch II region could be made (Feltham et al., 1997). However, in the NMR structure parts of the switch II region were left unassigned precluding a detailed comparison with the crystal structure. Because the observed differences in the switch II region between inactive and active conformations are quite small, no large conformational change in the switch II region of Rho/Rac/Cdc42 upon GTP hydrolysis is expected. Since the sequence of this region is completely conserved between Rac, Rho, and Cdc42, it is likely that the observed differences are due to the intrinsic flexibility of this region, which has been observed for the switch II region in Ras by both X-ray crystallography and NMR (Milburn et al., 1990; Pai et al., 1990; Kraulis et al., 1994) as well as for the switch II region of Cdc42 in both nucleotide states in solution (Feltham et al., 1997).

Discussion

In this paper, we describe the crystal structures of Cdc42(G12V) in complex with GDP/Mg^{2+} and $GDPNH_2$, which were obtained by serendipity from Cdc42(G12V)·GppNHp. An attempt was made to correlate the structural differences between the two molecules in the asymmetric unit with biochemical data about nucleotide affinity and kinetic behavior. An alteration of the crystal composition like seen with Cdc42(G12V) is not uncommon as for instance in the structure of the regulatory GTPase Rap2A (Cherfils et al.,

1997). GTP was found to reside in the active site although a GDP-complex was set up for crystallization. Contaminating kinase activity from *Escherichia coli* was made responsible for the phosphoryltransfer reaction. In the case of Cdc42(G12V), GppNHp was degraded to GDP and $GDPNH_2$ as found from HPLC analysis of the crystals.

The question arises why it has been possible to obtain crystals of Ras and other GTP-binding proteins in complex with GppNHp. One difference might have been the fact that most crystals of small GTPases have been grown around neutral pH, which probably stabilizes the protein and slows down the spontaneous hydrolysis of GppNHp. The other difference between the standard Ras·GppNHp crystallization conditions and the conditions used for Cdc42(G12V) is the presence of high concentrations of Li_2SO_4 compared to low salt concentrations for Ras (Scherer et al., 1989). The effect of the salt is indeed important as exemplified by the more than 30-fold increased dissociation rate constants k_{diss} of the fluorescent nucleotides mGDP and mGppNHp from the complex with Cdc42(G12V) in the presence of 0.3 M Li_2SO_4 as compared to the absence of Li_2SO_4. The influence of the Li_2SO_4 on nucleotide binding is therefore expected to be similar to $(NH_4)_2SO_4$, which is known to accelerate the nucleotide exchange in small GTPases considerably (John et al., 1990). Therefore, under the conditions of high salt concentrations and low pH, crystallization has to effectively compete with hydrolysis to explain the observed GDP and $GDPNH_2$ in the crystals, otherwise the GDP and $GDPNH_2$ would have been degraded as well. Once the Cdc42(G12V)·nucleotide complex is incorporated into the crystal, it seems not to be amenable to side reactions any more.

Due to different conformations of the effector loop, the Mg^{2+} coordination in Cdc42(G12V)·GDP looks more like in Ras·GDP than in RhoA·GDP, indicating that the mode of Mg^{2+} binding can be quite different within the group of the Rho-family proteins. The flexibility in binding is supported by the fact that the Mg^{2+} has an apparent equilibrium dissociation constant in the micromolar range and is in fast equilibrium with the solvent, dissociating also independently of the nucleotide (John et al., 1993; Leonard et al., 1994; M. Rudolph, unpubl. obs.). The most consistent feature of the Mg^{2+} binding site in GTP-binding proteins seems to be a monodentate coordination to the β-phosphate oxygen of GDP and a bidentate coordination to the β,γ-phosphate oxygens in the triphosphate structures, but the details of the coordination vary.

The Cdc42(G12V)·$GDPNH_2$ complex does not show density for a Mg^{2+} ion and apparently has a very much lower affinity for Mg^{2+} than the Cdc42(G12V)·GDP complex. Substituting an amino group for a negatively charged oxygen atom not only inverts the hydrogen bonding capability but also reduces the negative charge on the β-phosphate. The less negative potential of the β-phosphoramidate in $GDPNH_2$ could very well explain a decreased affinity of $GDPNH_2$ for Mg^{2+} as shown by fluorescence and thus the lacking density for a Mg^{2+} in the Cdc42(G12V)·$GDPNH_2$ structure. $GDPNH_2$ could prove as an interesting GDP analogue that like GDPβS could be useful for mechanistic studies such as the Mg^{2+} dependence of phosphoryl transfer reactions or the inhibition of G-proteins.

On comparing the overall structure of Cdc42(G12V)·GDP with RhoA·GDP (Wei et al., 1997) and Rac1·GppNHp (Hirshberg et al., 1997), it is apparent that the conformations of the insert regions are strikingly similar. Given the high degree of sequence identity within the insert regions, it can be assumed that they do not change their structures during the conformational switch from the GTP to the GDP form (Ihara et al., 1998). This is in line with the fact that apart from the insert region other regions on Rac1 contribute to the nucleotide specific binding of certain effectors such as the NADPH oxidase subunit $p67^{phox}$ (Freeman et al., 1996). Similarly, the insert region of Cdc42 was shown to be essential for the inhibition of nucleotide dissociation by RhoGDI, but not for the binding of the two proteins (Wu et al., 1997). It seems, therefore, that the insert region specific for the Rho proteins serves a regulatory role in the binding of certain subsets of target proteins rather than to specifically discriminate between them. Such discrimination is brought about by the switch regions and probably helix α3. It is known for example that the N-terminal part of helix α3 is involved in a major interaction with the Cdc42-GAP protein RhoGAP (Rittinger et al., 1997a) and it is thus tempting to assume that the looped-out conformation of Glu95 found in the Cdc42(G12V)·GDP structure might have a function in GAP binding or discrimination.

Most three-dimensional structures of Ras-related proteins have been solved with truncated proteins constituting the actual G-domain, leaving out the C-terminal region required for posttranslational modification and membrane attachment. In cases where full length proteins were present in the crystals, the C-terminal end was found to be disordered (Milburn et al., 1990; Pai et al., 1990; Scheffzek et al., 1995; Hirshberg et al., 1997; Wei et al., 1997). From these structures and biochemical studies comparing full-length vs. truncated proteins (John et al., 1989), it has been assumed that the only role of the C-terminal end, except for Ran, is to provide a flexible tail that after posttranslational modification is responsible for anchoring the protein into the particular membrane compartment required for its biological role. This is supported by the fact that the C-terminal end of Cdc42(G12V) is, even in the presence of a disulfide bond, still only partially visible in the electron density.

Materials and methods

Protein production and purification

The plasmid harboring the gene for the G12V mutant (Cdc42(G12V)) of the human placental Cdc42 protein was kindly provided by George Martin, Onyx Pharmaceuticals. Production of Cdc42(G12V) fused to glutathione-S-transferase and purification of the Cdc42·nucleotide complex have been reported (Rudolph et al., 1998). After cleavage of the fusion protein with thrombin, three additional amino acid residues (Gly-Ser-Pro) preceded the starting methionine at the N-terminus of Cdc42(G12V) as confirmed by protein sequencing. The integrity of the C-terminus was verified by mass spectrometry.

Fluorescence studies

Fluorescence measurements were done at 25 °C on a Fluoromax™ spectrofluorimeter (SPEX Instruments S.A., Inc., Edison, New Jersey). Titration of nucleotide-free Cdc42(G12V) with $GDPNH_2$ was performed in 40 mM HEPES/NaOH pH 7.4, 100 mM NaCl, 5 mM $MgCl_2$ with an automatic titrator using a Hamilton syringe as reservoir for the nucleotide. The decrease in fluorescence at 328 nm (8 nm bandwidth) was followed after excitation at 295 nm (0.2 nm bandwidth). Equilibrium dissociation constants were obtained by fitting the solution of a quadratic equation describing a

bimolecular association model assuming a 1:1 stoichiometry to the data. The influence of Li_2SO_4 on the nucleotide dissociation rate was measured as follows: Cdc42(G12V) complexed with mant-labeled nucleotides was diluted to 0.1 μM into 100 mM HEPES/NaOH pH 7.4, 300 mM Li_2SO_4, 0.5 mM $MgCl_2$. Dissociation of the fluorescent nucleotides was initiated by addition of a 1,000-fold excess of unlabeled nucleotide. The decrease in fluorescence at 435 nm (2 nm bandwidth) after excitation at 366 nm (0.3 nm bandwidth) was followed. For measurement of the dissociation of unlabeled nucleotides from Cdc42(G12V), ca. 0.1 μM of complex was added to excess (4.2–5 μM) mant-nucleotide in 40 mM HEPES/NaOH pH 7.4, 100 mM NaCl, 5 mM $MgCl_2$ and the increase in mant-fluorescence at 435 nm (4 nm bandwidth) due to energy transfer was followed after excitation of protein fluorescence at 295 nm (0.3 nm bandwidth). The association constant of mGDP for nucleotide free Cdc42(G12V) was measured using the same readout. Increasing concentrations of mGDP (0.5–6.5 μM final concentration) were mixed with nucleotide free Cdc42(G12V) (0.1 μM final concentration) at 25 °C in 40 mM HEPES/NaOH pH 7.4, 100 mM NaCl, 5 mM $MgCl_2$ in a stopped flow machine (Applied Photophysics, Leatherhead, United Kingdom) with the monochromators set to 1.5 nm and a cut-off filter of 408 nm. Single exponentials were fitted to all kinetic data using the program Grafit (Erithacus Software, Staines, United Kingdom). Linear regression of the apparent association rate constants as a function of mGDP-concentration yielded the microscopic association rate constant k_{ass}.

Crystallization, crystal analysis, and data collection

Tetragonal crystals were grown at 15 °C using the hanging drop method by mixing 1.5 μL of a 4 mM solution of Cdc42(G12V)·GppNHp in 20 mM HEPES/NaOH pH 7.4, 1 mM $MgCl_2$ with 1.5 μL reservoir solution consisting of 0.1 M NaOAc pH 4.7, 5% PEG 4000, and 0.3 M Li_2SO_4. Crystals were frozen after serial transfer to cryosolutions containing 0.1 M NaOAc pH 4.7, 10% PEG 4000, 0.3 M Li_2SO_4, and 5, 10, 15, and 20% glycerol, respectively.

A 100 K native data set was collected from a single crystal on beamline X31 at EMBL c/o DESY at a wavelength of 1.0774 Å using a MAR imaging plate scanner operating in 18 cm mode. Crystal to detector distance was 100 mm. Data reduction and processing were done using the DENZO/SCALEPACK program package (Otwinowski & Minor, 1997). The data statistics are given in Table 1.

The nature of the cofactors in the crystals was analyzed by isocratic HPLC (Tucker et al., 1986) on a C18 reversed phase column (Bischoff, Leonberg, Germany) using 0.1 M potassium phosphate pH 6.5, 10 mM tetrabutylammonium bromide, 0.2 mM NaN_3, 7.5% acetonitrile as the mobile phase. The absorption detector was set to 254 nm. Crystals survived washing several times with water and were dissolved in the above solution.

Structure determination and refinement

Because the interpretation of systematic absences was ambiguous, the space group was determined to be either $P4_122$, $P4_12_12$, $P4_322$, or $P4_32_12$. The Matthews parameter indicated two or three molecules in the asymmetric unit (V_m = 2.9 or 2.0, respectively).

Thus, a molecular replacement search using AMORE (CCP4, 1994) was performed in space groups $P4_122$, $P4_12_12$, $P4_322$, and $P4_32_12$ with two and three molecules to search for. Since at the stage of structure determination no coordinates of Rho-family proteins were available, the Ras·GDP and Ras·GppNHp complexes (PDB accession numbers 4q21 and 5p21, respectively) either as are or with their loops successively truncated were used as search models. Additionally, all models were used with either no changes of the side chains, all nonconserved residues changed to Ala or as poly-Ala. The results from AMORE were analyzed automatically for steric overlap of the transformed models using a fast packing analysis program (I. Vetter, unpubl. obs.). For this, the transformed models were approximated by a sphere encompassing 80% of their radius and the overlapping radii were calculated. The remaining solutions with the largest difference in correlation coefficients and *R*-factors between the first and second (best false) solution were visually checked for packing consistency. For poly-Ala Ras·GDP a solution was found for two molecules in space group $P4_12_12$. The difference in rotation angle for the two solutions matches the

Table 1. *Crystal parameters, data collection, and refinement statistics*

Crystal parameters	
Unit cell (a, c) (Å)	98.65, 104.16
Data statistics	
Resolution (Å)	30–2.5
Collected reflections	88,071
Unique reflections	18,254
Completeness (total/high) (%)[a]	99.3/99.9
R_m (total/high) (%)[b]	4.9/46.0
$\langle I/\sigma(I)\rangle$ (total/high)	15.6/3.3
Molecular replacement	
Search model	Poly-Ala Ras·GDP
Resolution range rotation (Å)	10-5
Resolution range translation (Å)	9-3
Correlation coefficient/*R*-factor (1^{st}, 2^{nd} peak) (%)	49.7/50.3, 41.3/54.2
Refinement statistics	
Resolution range (Å)	30–2.5
Reflections (2σ cut-off)	17,611
Protein atoms	3,098
Water	65
Others[c]	57
Bulk solvent (k, B) (e/Å^3, Å^2)	0.33/52.4
R_{cryst}/R_{free} (%)[d]	22.5/28.0
Stereochemical parameters	
RMSD bonds/angles (Å,°)	0.007/1.2
$\langle B\rangle$ mc first/second molecule (Å^2)[e]	46.9/66.1
$\langle B\rangle$ sc first/second molecule (Å^2)[e]	49.3/67.1
$\langle B\rangle$ GDP (Å^2)[e]	35.2
B Mg^{2+} (Å^2)[e]	39.9
$\langle B\rangle$ GDPNH$_2$ (Å^2)[e]	62.8
Mean coordinate error (Å)[f]	0.39

[a] Completeness, R_m and $\langle I/\sigma(I)\rangle$ are given for all data and those in the highest resolution shell (2.6–2.5 Å).
[b] $R_m = \Sigma|I - \langle I\rangle|/\Sigma I$.
[c] Other atoms correspond to one Mg^{2+}, one GDP and one GDPNH$_2$ in the asymmetric unit.
[d] $R_{cryst} = \Sigma||F_o| - |F_c||/\Sigma|F_o|$.
[e] Mean values are given for main chain (mc) and side chain (sc) atoms.
[f] According to Luzzati (1952).

position of a noncrystallographic peak in the $\kappa = 180^\circ$ section of the self-rotation function, which is consistent with a dimer in the asymmetric unit.

Because the molecular replacement solution from AMORE for the second molecule was much weaker than for the first one, separate cross rotation function searches using POLARRFN (CCP4, 1994), and subsequent translation searches using TFFC (CCP4, 1994) were performed. The same solution as from AMORE for the first molecule, but not the second molecule was obtained. After rigid body refinement of the secondary structure elements of the first molecule using TNT (Tronrud, 1997), the translation for the second molecule was found after rotating this molecule around the axis corresponding to the noncrystallographic twofold and using it as input in TFFC. This resulted in a translation that was offset by about 4 Å from the AMORE solution and turned out to be the correct one.

The starting model for the refinement was the asymmetric unit containing two coordinate sets of Ras in the GDP-conformation without the nucleotide, all loops omitted and the remaining residues mutated to Ala. X-PLOR 3.851 (Brünger, 1992b) and DM (CCP4, 1994) were used for all refinement and density modification calculations. Map interpretation and manual rebuilding were done using the graphics program O (Jones et al., 1991). The refinement strategy was as follows: Initial rigid body refinement of the two molecules was followed by a simulated annealing refinement using the "slowcool" protocol (Brünger et al., 1990) starting at 3,000 K to remove model bias. Strong NCS constraints were used throughout. The resulting model was subjected to density modification using DM with solvent flattening, histogram matching, and NCS averaging. After a few rounds of subsequent rebuilding and refinement, no further improvement of the model was achieved. Following this, the refinement protocol in X-PLOR was changed to an initial positional refinement followed by a 3,000 K simulated annealing refinement and careful individual *B*-factor refinement using the free *R*-factor as a monitor for model quality. An additional torsion angle refinement (Brünger, 1992a; Jiang & Brünger, 1994) starting at 10,000 K lowered the free *R*-factor by 1%. Solvent flattening and histogram matching but no NCS averaging were used in DM at this stage and since then the strict asymmetry of the nucleotide binding sites of the noncrystallographic dimer became apparent. A two parameter bulk solvent correction (Jiang & Brünger, 1994) was applied in the final stages of refinement and recalculated after each round of rebuilding. Since the two molecules in the asymmetric unit are discussed separately, they are referred to as first (residue number 1 to 200) and second (201 to 400) molecule. The three artificial N-terminal residues (Gly-Ser-Pro) and two C-terminal residues (Leu191 and Leu391) were not visible in the electron density and, therefore, omitted from the model. Other residues (Pro180 to Lys183 in molecule 1, and Ser230 to Asp238, Gly260 to Arg266, Glu327 to Lys335, Pro380 to Lys384, Val389 to Leu390 in molecule 2), which did not show interpretable density were modeled according to stereochemical constraints and excluded from the NCS restraints. As turned out during the refinement, the second molecule is less well defined than the first and has *B*-factors that are on the average 1.4-fold higher (Table 1). The final model consists of two molecules of Cdc42(G12V) bound to GDP/Mg^{2+} and $GDPNH_2$, respectively, and was refined to a free *R*-factor of 28% (Table 1); 98.8 and 1.2% of the nonglycine residues are in the most favored and additionally allowed regions of the Ramachandran plot, respectively (Laskowski et al., 1993). The atomic coordinates and structure factors of the asymmetric unit have been deposited at the Protein Data Bank, accession code 1a4r.

Acknowledgments

We thank Arnon Lavie, Balaji Prakash, Louis Renault, Klaus Scheffzek, and Ilme Schlichting for discussions, Michael Hess for help with the figures, and Rita Schebaum for secretarial assistance. The expert help from the staff at the EMBL-outstation Hamburg is gratefully acknowledged, and we thank EMBL for beam time.

References

Ahmadian MR, Stege P, Scheffzek K, Wittinghofer A. 1997. Confirmation of the arginine-finger hypothesis for the GAP-stimulated GTP-hydrolysis reaction of Ras. *Nat Struct Biol 4*:686–689.

Best A, Ahmed S, Kozma R, Lim L. 1996. The Ras-related GTPase Rac1 binds tubulin. *J Biol Chem 271*:3756–3762.

Bourne HR, Sanders DA, McCormick F. 1990. The GTPase superfamily: A conserved switch for diverse cell functions. *Nature 348*:125–132.

Brünger AT. 1992a. Free *R* value: A novel statistical quantity for assessing the accuracy of crystal structures. *Nature 355*:472–474.

Brünger AT. 1992b. *X-PLOR Version 3.1: A system for X-ray crystallography and NMR*. New Haven, CT: Yale University Press.

Brünger AT, Krukowski A, Erickson JW. 1990. Slow-cooling protocols for crystallographic refinement by simulated annealing. *Acta Cryst A46*:585–593.

Cherfils J, Menetrey J, Le Bras G, Janoueix-Lerosey I, de Gunzburg J, Garel JR, Auzat I. 1997. Crystal structures of the small G protein Rap2A in complex with its substrate GTP, with GDP and with GTPγS. *EMBO J 16*:5582–5591.

Collaborative Computational Project Number 4. 1994. The CCP4 Suite: Programs for protein crystallography. *Acta Cryst D50*:760–763.

Connolly ML. 1993. The molecular surface package. *J Mol Graphics 11*:139–141.

Esnouf RM. 1997. An extensively modified version of Molscript that includes greatly enhanced coloring capabilities. *J Mol Graphics 15*:132–134.

Fauman EB, Saper MA. 1996. Structure and function of the protein tyrosine phosphatases. *TIBS 21*:413–417.

Feltham JL, Dotsch V, Raza S, Manor D, Cerione RA, Sutcliffe MJ, Oswald RE. 1997. Definition of the switch surface in the solution structure of Cdc42Hs. *Biochemistry 36*:8755–8766.

Franken SM, Scheidig AJ, Krengel U, Rensland H, Lautwein A, Geyer M, Scheffzek K, Goody RS, Kalbitzer HR, Pai EF, Wittinghofer A. 1993. Three-dimensional structures and properties of a transforming and a nontransforming glycine-12 mutant of $p21^{H\text{-}ras}$. *Biochemistry 32*:8411–8420.

Freeman JL, Abo A, Lambeth JD. 1996. Rac insert region is a novel effector region that is implicated in the activation of NADPH oxidase but not PAK65. *J Biol Chem 271*:19794–19801.

Hirshberg M, Stockley RW, Dodson G, Webb MR. 1997. The crystal structure of human Rac1 a member of the Rho-family complexed with a GTP analogue. *Nat Struct Biol 4*:147–152.

Huang W, Jia J, Edwards P, Dehesh K, Schneider G, Lindqvist Y. 1998. Crystal structure of β-ketoacyl-carrier protein synthase II from *E. coli* reveals the molecular architecture of condensing enzymes. *EMBO J 17*:1183–1191.

Ihara K, Muraguchi S, Kato M, Shimizu T, Shirakawa M, Kuroda S, Kaibuchi K, Hakoshima T. 1998. Crystal structure of human RhoA in a dominantly active form complexed with a GTP analogue. *J Biol Chem 273*:9656–9666.

Jiang JS, Brünger AT. 1994. Protein hydration observed by X-ray diffraction. Solvation properties of penicillopepsin and neuraminidase crystal structures. *J Mol Biol 243*:100–115.

John J, Frech M, Wittinghofer A. 1988. Biochemical properties of Ha-ras encoded p21 mutants and mechanism of the autophosphorylation reaction. *J Biol Chem 263*:11792–11799.

John J, Rensland H, Schlichting I, Vetter I, Borasio GD, Goody RS, Wittinghofer A. 1993. Kinetic and structural analysis of the Mg^{2+}-binding site of the guanine nucleotide-binding protein $p21^{H\text{-}ras}$. *J Biol Chem 268*:923–929.

John J, Schlichting I, Schiltz E, Rösch P, Wittinghofer A. 1989. C-terminal truncation of $p21^{H\text{-}ras}$ preserves crucial kinetic and structural properties. *J Biol Chem 264*:13086–13092.

John J, Sohmen R, Feuerstein J, Linke R, Wittinghofer A, Goody RS. 1990. Kinetics of interaction of nucleotides with nucleotide free H-ras p21. *Biochemistry 29*:6058–6065.

Jones TA, Zou JY, Cowan SW, Kjeldgaard M. 1991. Improved methods for

building protein models in electron density maps and the location of error in these models. *Acta Cryst A47*:110–119.

Kortemme T, Creighton TE. 1995. Ionisation of cysteine residues at the termini of model α-helical peptides. Relevance to unusual thiol pK_a values in proteins of the thioredoxin family. *J Mol Biol 253*:799–812.

Kraulis PJ. 1991. MOLSCRIPT—A program to produce both detailed and schematic plots of protein structures. *J Appl Cryst 24*:946–950.

Kraulis PJ, Domaille PJ, Campbell-Burk SL, Van Aken T, Laue ED. 1994. Solution structure and dynamics of rasp21.GDP determined by heteronuclear three- and four-dimensional NMR spectroscopy. *Biochemistry 33*:3515–3531.

Krengel U, Schlichting I, Scherer A, Schumann R, Frech M, John J, Kabsch W, Pai EF, Wittinghofer A. 1990. Three dimensional structures of H-ras p21-mutants: Molecular basis for their inability to function as signal switch molecules. *Cell 62*:539–548.

Lancaster CA, Taylor-Harris PM, Self AJ, Brill S, van Erp HE, Hall A. 1994. Characterization of rhoGAP. A GTPase-activating protein for rho-related small GTPases. *J Biol Chem 269*:1137–1142.

Laskowski RA, MacArthur MW, Moss DS, Thornton JM. 1993. PROCHECK—A program to check the stereochemical quality of proteins. *J Appl Cryst 26*:283–291.

Leonard DA, Evans T, Hart M, Cerione RA, Manor D. 1994. Investigation of the GTP-binding/GTPase cycle of Cdc42Hs using fluorescence spectroscopy. *Biochemistry 33*:12323–12328.

Li R, Zheng Y. 1997. Residues of the Rho family GTPases Rho and Cdc42 that specify sensitivity to DBL-like guanine nucleotide exchange factors. *J Biol Chem 272*:4671–4679.

Luzzati V. 1952. Traitement statistique des erreurs dans la determination des structures cristallines. *Acta Cryst 5*:802–810.

Matsui T, Amano M, Yamamoto T, Chihara K, Nakafuku M, Ito M, Nakano T, Okawa K, Iwamatsu A, Kaibuchi K. 1996. Rho-associated kinase a novel serine/threonine kinase as a putative target for the small GTP binding protein Rho. *EMBO J 15*:2208–2216.

McCallum SJ, Wu WJ, Cerione RA. 1996. Identification of a putative effector for Cdc42Hs with high sequence similarity to the RASGAP-related protein IQGAP1 and a Cdc42Hs binding partner with similarity to IQGAP2. *J Biol Chem 271*:21732-21737.

Merrit EA, Bacon DJ. 1997. Raster3D: Photorealistic molecular graphics. *Methods Enzymol 277*:505–524.

Milburn MV, Tong L, DeVos AM, Brünger A, Yamaizumi Z, Nishimura S, Kim SH. 1990. Molecular switch for signal transduction: Structural differences between active and inactive forms of protooncogenic *ras* proteins. *Science 247*:939–945.

Nassar N, Horn G, Herrmann C, Block C, Janknecht R, Wittinghofer A. 1996. Ras/Rap effector specificity determined by charge reversal. *Nat Struct Biol 3*:723–729.

Nassar N, Horn G, Herrmann C, Scherer A, McCormick F, Wittinghofer A. 1995. The 2.2 Å crystal structure of the Ras-binding domain of the serine/threonine kinase c-Raf1 in complex with Rap1A and a GTP analogue. *Nature 375*:554–560.

Nicholls A, Sharp KA, Honig B. 1991. Protein folding and association: Insights from the interfacial and thermodynamic properties of hydrocarbons. *Proteins 11*:281–293.

Nobes CD, Hall A. 1995. Rho Rac and Cdc42 GTPases regulate the assembly of multimolecular focal complexes associated with actin stress fibers lamellipodia and filopodia. *Cell 81*:53–62.

Olson MF, Pasteris NG, Gorski JL, Hall A. 1996. Faciogenital dysplasia protein (FGD1) and VAV two related proteins required for normal embryonic development are upstream regulators fo Rho GTPases. *Curr Biol 6*:1628–1633.

Otwinowski Z, Minor W. 1997. Processing of X-ray diffraction data collected in oscillation mode. *Methods Enzymol 276*:307–327.

Pai EF, Krengel U, Petsko GA, Goody RS, Kabsch W, Wittinghofer A. 1990. Refined crystal structure of the triphosphate conformation of H-*ras* p21 at 1.35Å resolution: Implications for the mechanism of GTP hydrolysis. *EMBO J 9*:2351–2359.

Qiu RG, Abo A, McCormick F, Symons M. 1997. Cdc42 regulates anchorage-independent growth and is necessary for Ras transformation. *Mol Cell Biol 17*:3449–3458.

Quilliam LA, Lambert QT, Mickelson-Young LA, Westwick JK, Sparks AB, Kay BK, Jenkins NA, Gilbert DJ, Copeland NG, Der CJ. 1996. Isolation of a NCK-associated kinase PRK2 an SH3-binding protein and potential effector of Rho protein signaling. *J Biol Chem 271*:28772–28776.

Rensland H, John J, Linke R, Simon I, Schlichting I, Wittinghofer A, Goody RS. 1995. Substrate and product structural requirements for binding of nucleotides to H-ras p21: The mechanism of discrimination between guanosine and adenosine nucleotides. *Biochemistry 34*:593–599.

Rittinger K, Walker PA, Eccleston JF, Nurmahomed K, Owen D, Laue E, Smerdon SJ. 1997a. Crystal structure of a small G protein in complex with the GTPase-activating protein RHOGAP. *Nature 388*:693–697.

Rittinger K, Walker PA, Eccleston JF, Smerdon SJ, Gamblin SJ. 1997b. Structure at 1.65 Å of RHOA and its GTPase-activating protein in complex with a transition-state analogue. *Nature 389*:758–762.

Rudolph MG, Bayer P, Abo A, Kuhlmann J, Vetter IR, Wittinghofer A. 1998. The CRIB motif of the Wiskott Aldrich syndrome protein WASP is necessary but not sufficient for tight binding to Cdc42 and structure formation. *J Biol Chem 273*:18067–18076.

Scheffzek K, Klebe C, Fritz-Wolf K, Kabsch W, Wittinghofer A. 1995. Crystal structure of the nuclear Ras-related protein Ran in its GDP-bound form. *Nature 374*:378–381.

Scherer A, John J, Linke R, Goody RS, Wittinghofer A, Pai EF, Holmes KC. 1989. Crystallization and preliminary X-ray analysis of the human c-H-*ras*-oncogene product p21 complexed with GTP analogues. *J Mol Biol 206*:257–259.

Sondek J, Shortle D. 1990. Accommodation of single amino acid insertions by the native state of staphylococcal nuclease. *Proteins 7*:299–305.

Tong L, de Vos AM, Milburn MV, Kim SH. 1991. Crystal structures at 2.2 Å resolution of the catalytic domains of normal ras protein and an oncogene mutant complexed with GDP. *J Mol Biol 217*:503–516.

Tronrud DE. 1997. TNT refinement package. *Methods Enzymol 277*:306–319.

Tucker J, Sczakiel G, Feuerstein J, John J, Goody RS, Wittinghofer A. 1986. Expression of p21 proteins in *Escherichia coli* and stereochemistry of the nucleotide-binding site. *EMBO J 5*:1351–1358.

Vetter IR, Baase WA, Heinz DW, Xiong JP, Snow S, Matthews BW. 1996. Protein structural plasticity exemplified by insertion and deletion mutants in T4 lysozyme. *Protein Sci 5*:2399–2415.

Wei Y, Zhang Y, Derewenda U, Liu X, Minor W, Nakamoto RK, Somlyo AV, Somlyo AP, Derewenda ZS. 1997. Crystal structure of RhoA-GDP and its functional implications. *Nat Struct Biol 4*:699–703.

Wu WJ, Leonard DA, Cerione RA, Manor D. 1997. Interaction between Cdc42Hs and RhoGDI is mediated through the Rho insert region. *J Biol Chem 272*:26153–26158.